Molecular Cancer Therapeutics

Establishment of the *InVivo* Efficacy of Pretargeted Radioimmunotherapy Utilizing Inverse Electron Demand Diels-Alder Click Chemistry

Jacob L. Houghton[1,2], Rosemery Membreno[3,4], Dalya Abdel-Atti[1,2], Kristen M. Cunanan[5], Sean Carlin[1], Wolfgang W. Scholz[6], Pat B. Zanzonico[7], Jason S. Lewis[1,2,8], and Brian M. Zeglis[1,3,4,8]

Abstract

The pretargeting system based on the inverse electron demand Diels-Alder reaction (IEDDA) between *trans*-cyclooctene (TCO) and tetrazine (Tz) combines the favorable pharmacokinetic properties of radiolabeled small molecules with the affinity and specificity of antibodies. This strategy has proven to be an efficient method for the molecularly targeted delivery of pharmaceuticals, including isotopes for radiological imaging. Despite encouraging results from *in vivo* PET imaging studies, this promising system has yet to be thoroughly evaluated for pretargeted radioimmunotherapy (PRIT). Toward that end, we synthesized two novel ^{177}Lu-labeled tetrazine-bearing radioligands. Next, we compared the usefulness of our ligands for PRIT when paired with TCO-modified 5B1—a human, anti-CA19.9 mAb—in preclinical murine models of pancreatic cancer. The exemplary ligand, ^{177}Lu-DOTA-PEG$_7$-Tz, showed rapid (4.6 ± 0.8% ID/g at 4 hours) and persistent (16.8 ± 3.9% ID/g at 120 hours) uptake in tumors while concurrently clearing from blood and nontarget tissues. Single-dose therapy studies using 5B1-TCO and varying amounts of ^{177}Lu-DOTA-PEG$_7$-Tz (400, 800, and 1,200 μCi) showed that our system elicits a dose-dependent therapeutic response in mice bearing human xenografts. Furthermore, dosimetry calculations suggest that our approach is amenable to clinical applications with its excellent dosimetric profile in organs of clearance (i.e., liver and kidneys) as well as in dose-limiting tissues, such as red marrow. This study established that a pretargeted methodology utilizing the IEDDA reaction can rapidly and specifically deliver a radiotherapeutic payload to tumor tissue, thus illustrating its excellent potential for clinical translation. *Mol Cancer Ther; 16(1); 124–33. ©2016 AACR.*

Introduction

For over three decades, the remarkable selectivity and affinity of antibodies for tumor biomarkers have made them attractive vectors for the selective delivery of therapeutic radiation to cancer cells (1, 2). A wide variety of antibodies have been labeled with a range of therapeutic isotopes. Indeed, a number of therapeutic radioimmunoconjugates are currently the subject of clinical trials, and two constructs—^{90}Y-ibritumomab tiuxetan and ^{131}I-tositumomab—have been approved for the treatment of non-Hodgkin lymphoma (3, 4). However, an important limitation compromising targeted radioimmunotherapy (RIT) is that immunoglobulins can take multiple days to reach their optimal biodistribution *in vivo*. This relatively slow pharmacokinetic profile mandates the use of therapeutic isotopes with long physical half-lives, such as ^{90}Y ($t_{1/2}$ ∼ 2.7 days), ^{177}Lu ($t_{1/2}$ ∼ 6.6 days), and ^{131}I ($t_{1/2}$ ∼ 8.0 days). This combination of slow pharmacokinetics, long physical half-lives, and therapeutic radiation can potentially result in prohibitively high radiation doses to healthy organs, particularly bone marrow (5). An effective radioimmunoconjugate must therefore strike a balance between delivering a therapeutic dose of radiation to the tumor while avoiding, or at least minimizing, radiation-related side effects. This issue becomes particularly important in the context of solid lesions, for which effective RIT has long proven elusive due to slow uptake, radiation resistance, and poor tumor penetration (6, 7). In principle, these obstacles could be overcome by injecting higher activities; however, the suboptimal tumor-to-tissue activity concentration ratios of traditional radioimmunoconjugates often preclude this course, as dose-limiting radiation toxicities would be reached before effective therapy could be achieved.

In response to these issues, considerable attention has been dedicated to the creation of RIT strategies that reduce the radiation

[1]Department of Radiology, Memorial Sloan Kettering Cancer Center, New York, New York. [2]Program in Molecular Pharmacology, Memorial Sloan Kettering Cancer Center, New York, New York. [3]Department of Chemistry, Hunter College and the Graduate Center of the City University of New York, New York, New York. [4]Ph.D. Program in Chemistry of the Graduate Center of the City University of New York, New York, New York. [5]Department of Epidemiology and Biostatistics, Memorial Sloan Kettering Cancer Center, New York, New York. [6]MabVax Therapeutics, San Diego, California. [7]Department of Medical Physics, Memorial Sloan Kettering Cancer Center, New York, New York. [8]Weill Cornell Medical College, New York, New York.

Note: Supplementary data for this article are available at Molecular Cancer Therapeutics Online (http://mct.aacrjournals.org/).

Corresponding Author: Brian M. Zeglis, Hunter College of the City University of New York, 413 East 69th Street, 4th Floor, Room BB452, New York, NY 10021. Phone: 212-896-0443; Fax: 212-772-5332; E-mail: bz102@hunter.cuny.edu

doi: 10.1158/1535-7163.MCT-16-0503

burden to healthy tissues, most notably the development of radiolabeled antibody fragments (8, 9). Another promising approach is pretargeted radioimmunotherapy (PRIT; ref.10). The aim of PRIT is to harness the tumor-targeting properties of antibodies while avoiding their pharmacokinetic drawbacks by decoupling the targeting vector from the radioisotope. More specifically, PRIT strategies typically employ four steps (Fig. 1A): (i) the administration of an unlabeled antibody with the ability to bind both an antigen and a radioligand; (ii) the slow accumulation of the antibody in the tumor and its concomitant clearance from the blood; (iii) the subsequent administration of a small-molecule radioligand; and (iv) the rapid binding of the radioligand to the antibody at the tumor site and the rapid excretion of any excess radioligand. Administration of the radioisotope in the form of a small molecule with rapid pharmacokinetics rather than a large molecule (i.e., the antibody) with slow kinetics is the key feature of this paradigm. As a result, PRIT yields high activity concentrations in tumors while keeping radiation doses to healthy organs low. Until recently, three approaches to *in vivo* pretargeting have dominated the field: bispecific antibodies engineered to bind both an antigen and a radiolabeled hapten, streptavidin-labeled antibodies with biotin-based radioligands, and oligonucleotide-bearing antibodies with radioligands modified with complementary sequences. All three strategies have proven effective in preclinical studies, yet each has been limited somewhat by various obstacles, such as the immunogenicity of streptavidin-based immunoconjugates (11–15).

The past 5 years have witnessed the emergence of a new approach to *in vivo* pretargeting based on the inverse electron demand Diels-Alder (IEDDA) reaction between tetrazine (Tz) and

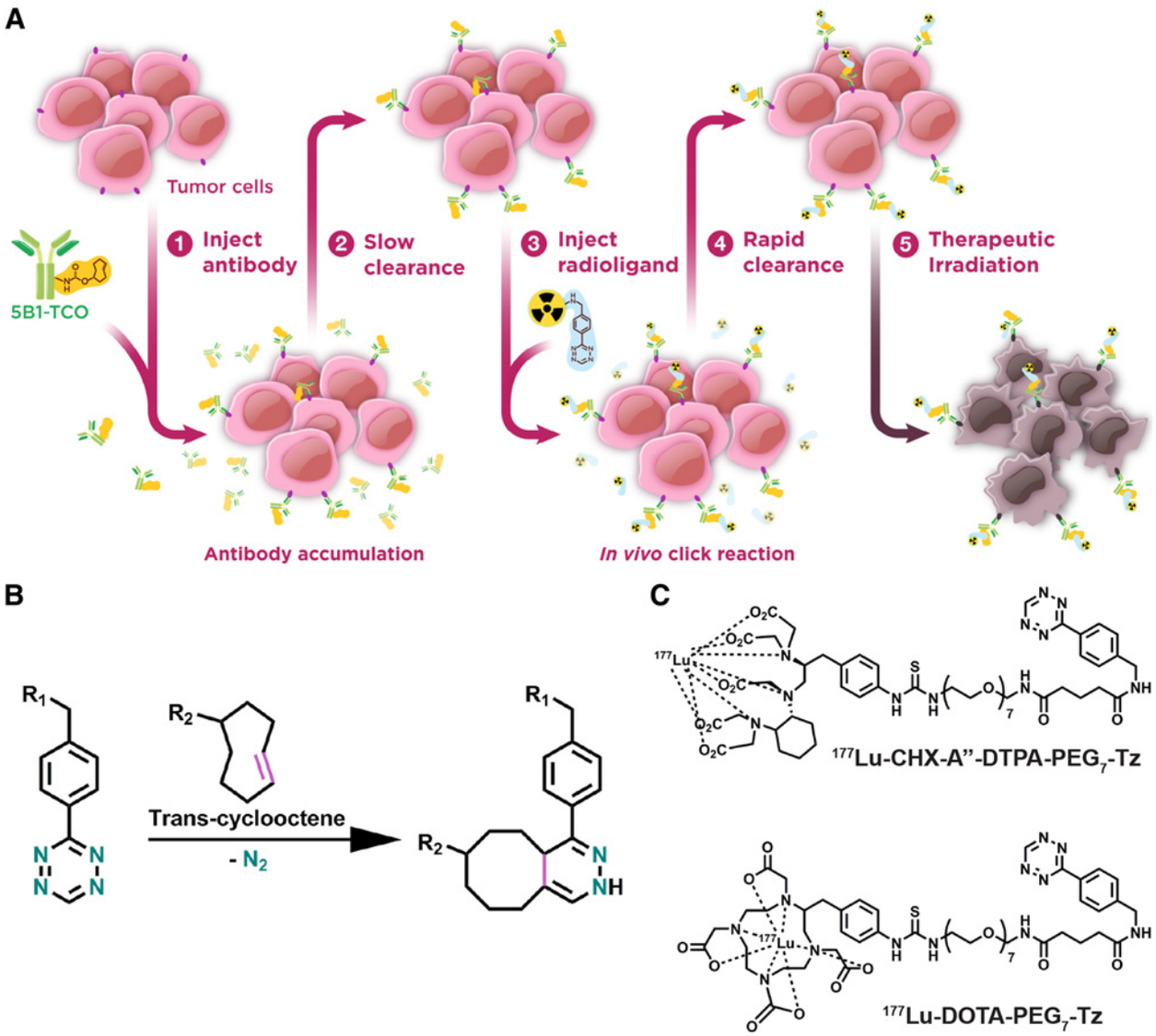

Figure 1.

A cartoon depicting the four basic steps of the pretargeted radioimmunotherapy approach used in these studies is shown (**A**). Also depicted is the reaction between the two components (TCO and Tz) on which the system is based (**B**) and the two ^{177}Lu-labeled ligands used in these studies (**C**).

trans-cyclooctene (TCO; Fig. 1B; refs.16, 17). This straightforward and modular methodology is predicated on the extraordinary selectivity and rapidity ($k_1 > 30{,}000\ M^{-1}s^{-1}$) of the bioorthgonal cycloaddition between a TCO-modified antibody and a tetrazine-bearing radioligand (Fig. 1A; refs.18–21). The earliest reports of this methodology focused on pretargeted SPECT imaging using an ^{111}In-labeled radioligand and a TAG72-targeting CC49-TCO immunoconjugate (22). More recently, our laboratories have developed highly effective pretargeted PET imaging strategies for both colorectal carcinoma and pancreatic ductal adenocarcinoma (PDAC) using ^{64}Cu- and ^{18}F-labeled tetrazine radioligands (23–25). In both cases, the pretargeting approaches identify tumor tissue extremely well, yielding images with high tumor-to-background contrast at only a fraction of the radiation dose produced by directly labeled radioimmunoconjugates. Given the success of these pretargeted imaging modalities, the logical next step is to leverage this technology for the development of a safe and effective approach to PRIT (26). Notably, although Rossin and colleagues have successfully demonstrated the feasibility of ^{177}Lu-based PRIT utilizing this methodology, to the best our knowledge no *in vivo* therapy studies have yet been published (27, 28).

In this article, we present the development, optimization, and *in vivo* validation of a pretargeted approach for the RIT of PDAC based on bioorthogonal click chemistry. We have used ^{177}Lu-labeled tetrazine radioligands (Fig. 1C) and a TCO-modified immunoconjugate of 5B1, a fully human antibody that targets the PDAC biomarker carbohydrate antigen 19.9 (CA19.9; refs.23, 24, 29–31). We demonstrate that this approach elicits a dose-dependent therapeutic response in mice bearing CA19.9-expressing BxPC3 human PDAC xenografts.

Materials and Methods

Cell lines and animal models

All studies were performed in accordance with Memorial Sloan Kettering Institutional Animal Care and Use Committee. All *in vivo* studies were carried out in female, athymic nude mice [Crl:NU(NCr)-Foxn1^{nu}, 6–8 weeks) bearing subcutaneous BxPC3 xenografts that were inoculated on the right flank, as previously described (29, 31). BxPC3 cells obtained from ATCC were obtained in November 2014, validated via STR analysis, and used within 4 weeks of resuscitation. BxPC3 cells were grown in RPMI medium modified to contain 4.5 g/L glucose, 1.5g/L sodium bicarbonate and supplemented with 10% (v/v) heat-inactivated FCS, 100 IU penicillin, 100 μg/mL streptomycin, 10 mmol/L HEPES, and 10 cc/L nonessential amino acids. Mice were xenografted subcutaneously with 5×10^6 cells, suspended in 150 μL of a solution containing a 1:1 mixture of Matrigel (Becton Dickinson), and cell culture medium. BxPC3 tumors were grown for 21 to 28 days postimplantation before imaging or biodistribution.

Preparation and characterization of 5B1-TCO

The *N*-hydroxysuccinyl ester of TCO [(*E*)-cyclooct-4-enyl 2,5-dioxo-1-pyrrolidinyl carbonate; TCO-NHS)] was conjugated to 5B1 as previously described (23). The average number of TCO molecules per antibody was estimated by incubating the 5B1-TCO with >150-fold excess of a Tz-functionalized Alexa Fluor 680 (Tz-AF680) and quantifying the ratio of Tz-AF680 per antibody, after purification by gel filtration, via UV-Vis as previously described (23–25). Further details are provided in the Supporting Information.

Synthesis and characterization of CHX-A″-DTPA-PEG$_7$-Tz (1) and DOTA-PEG$_7$-Tz (2)

Both DOTA-PEG$_7$-Tz and CHX-A″-DTPA-PEG$_7$-Tz were prepared via a three-step synthesis that is fully described in Supplementary Fig. S1. In short, a commercially available amine-reactive *N*-hydroxysuccinyl tetrazine (Tz-NHS) was coupled to a mono-Boc protected, bis-amino PEG$_7$ molecule to form Tz-PEG$_7$-NHBoc (1) which was subsequently deprotected in a mixture of methylene chloride and trifluoroacetic acid to form a common intermediate, Tz-PEG$_7$-NH$_2$ (2). Then, the *p*-isothiocyanate of DOTA or CHX-A-DTPA was coupled to yield the products; DOTA-PEG$_7$-Tz and CHX-A″-DTPA-PEG$_7$-Tz. All products and intermediates were characterized by ^{1}H-NMR (Supplementary Fig. S2), ^{13}C-NMR, ESI-MS, and high-resolution mass spectrometry (HR-MS).

Radiolabeling of DOTA-PEG$_7$-Tz and CHX-A″-DTPA-Tz

DOTA-PEG$_7$-Tz and CHX-A″-DTPA-Tz were radiolabeled (Supplementary Fig. S3) by diluting stock solution (10 mg/mL in DMSO) into ammonia acetate buffer (200 mmol/L, pH 5.4, 100 μL) prior to addition of $^{177}LuCl_3$ in a 0.05 mol/L HCl solution (0.5–5 μL). The labeling solution was incubated at room temperature for 20 minutes before quenching with EDTA (50 mmol/L, pH 5.5, 10 μL). The products were isolated via HPLC (0–100% MeCN, 15 minutes), and the solvent was removed on a rotary evaporator before reconstituting in 0.9% saline for injection.

Functional characterization of radioligands

The partition coefficient (log *D*) for both radioligands was determined in PBS and 1-octanol. In short, a small amount of radioligand (~100 μCi) was added to a 1:1 mixture of PBS and 1-octanol and the sample was vortexed for 10 minutes, and the layers separated by centrifugation (1,000 rpm for 10 minutes). The layers were then placed into separate tubes for quantification by gamma counting. In addition, the *in vitro* stability of each radioligand was analyzed in both PBS (pH 7.4) and human serum at 37°C up to 48 hours (Supplementary Table S1). Aliquots of radiolabeled ligands (1.0 mCi) were added to PBS or serum and incubated at 37°C. At various time points an aliquot was removed and analyzed by radio-iTLC. All experiments were performed in triplicate; additional details may be found in the Supplementary Information.

Biodistribution

Tumor-bearing mice were injected via the lateral tail vein with 5B1-TCO (100 or 200 μg). For all biodistribution studies, mice that received 5B1-TCO were administered 40–50 μCi of ^{177}Lu-DOTA-PEG$_7$-Tz or ^{177}Lu-CHX-A″-DTPA-Tz in an approximately 1.5:1 ratio of radioligand to 5B1-TCO (either 1 or 2 nmol), which was delivered 72 hours after administration of the 5B1-TCO (Fig. 2; Supplementary Fig. SI4–SI6; and Supplementary Table S2). In addition, one cohort was administered 1,200 μCi of ^{177}Lu-DOTA-PEG$_7$-Tz to ensure that increasing the specific activity did not cause a deviation in total the biodistribution (this method was established as the optimal dosing strategy based on the *in vivo* behavior of 5B1 in previous studies; refs.23, 24). Tissues were collected and analyzed as previously described between 4 and 120 hours. Further details are outlined in the supporting information.

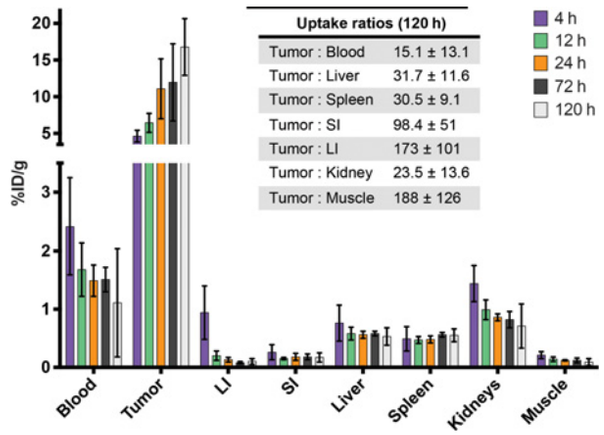

Figure 2.

Biodistribution data obtained from an *in vivo* pretargeting experiment in which ^{177}Lu-DOTA-PEG$_7$-Tz (2 nmol) was injected 72 hours after the administration of 5B1-TCO (1.3 nmol). The activity concentrations in selected tissues at time points ranging from 4 to 120 hours after the injection of ^{177}Lu-DOTA-PEG$_7$-Tz were determined along with selected tumor-to-tissue activity concentration ratios (inset).

Dosimetry

The biodistribution data for the ^{177}Lu-Tz-PEG$_7$-DOTA–based pretargeting system were expressed as normal-organ mean standard uptake values (SUV) versus time postadministration. Assuming, in first order, that SUVs are independent of body mass and thus the same among species, the mean SUV in mouse organ i, SUV_i, was converted to the fraction of the injected dose in the corresponding human organ I, FID_I, using the organ and total-body masses of the 70-kg Standard Man anatomic model and the following formula:

$$FID_I = SUV_i \bullet \frac{\text{Mass of Human Organ}_I}{\text{Mass of Human Total Body}}$$

These data (corrected for radioactive decay) were fit to exponential time–activity functions. The cumulated activity, or residence time, in human organ i (t_i, in μCi-h/μCi) was calculated by integrating the time–activity function in organ i, replacing the biological clearance constant, $(\lambda_b)_x$ for each component, x, of the fitted exponential function with the corresponding effective clearance constant, $(\lambda_e)_x$ [$(\lambda_e)_x = (\lambda_b)_x + \lambda_p$, where λ_p is the physical decay constant of the radionuclide]. The resulting organ residence times were entered into the OLINDA computer program to yield the mean organ absorbed doses and effective dose in rad/mCi and rem/mCi, respectively (Tables 1 and 2; ref.32).

In vivo therapy

Tumor volumes for all mice were determined via caliper measurements of the longest dimension (x) and shortest dimension (y) and using the equation tumor volume (mm^3) $= x/2 \times y^2$. After initial tumor measurements, mice were randomized into five cohorts (n = 7–8 per cohort), ensuring all cohort had approximately equal average tumor volumes. Seventy-two hours prior to administration of the radioligands, the three cohorts that were selected to receive therapy were administered 5B1-TCO (200 μg; 1.3 nmol), whereas the two control cohorts were administered vehicle only (0.9% sterile saline). Seventy-two hours later (day 1), the tumors dimensions were measured again, and those resulting volumes set as the initial tumor volumes to which the relative growth was compared throughout the study. Immediately after day 1 tumor measurements, mice in the therapy cohorts were then administered 400, 800, or 1,200 μCi of ^{177}Lu-DOTA-PEG$_7$-Tz (1.92 ± 0.06 nmol, 1.44 ± 0.05 Tz:mAb ratio). The control cohorts that had not been previously administered 5B1-TCO were injected with either vehicle (0.9% sterile saline) or 1,200 μCi of ^{177}Lu-DOTA-PEG$_7$-Tz (1.83 nmol). Tumor volume was monitored via caliper measurement every 3 to 7 days up to the predetermined endpoint of tumor volume (1,000 mm^3) or 51 days (Fig. 3). All mice were assessed twice per week throughout the study for outward signs of toxicity, including lethargy, loss of appetite, and decreasing body weight. The endpoint for individual mice was defined as the point at which the volume of the xenograft was measured to be ≥1,000 mm^3, and the study was terminated when 50% of both control groups had reached the predetermined endpoint.

PET imaging

^{89}Zr-DFO-5B1 (^{89}Zr-5B1) was prepared as previously described (29). For this study, mice that still harbored viable tumor tissue of approximately the same size (200–450 mm^3) were selected, including one from each control group and two each from the cohorts that received 800 or 1,200 μCi of radioligand in the *in vivo* PRIT study. The selected mice were injected with ^{89}Zr-5B1 (118 ± 3 μCi, ∼35 μg, ∼0.23 nmol), and PET images were acquired at 120 hours postinjection as previously described (Fig. 4A-B and Supplementary Fig. S7; refs.29, 31). Further details regarding image acquisition, reconstruction, and processing are provided in the Supplementary Information.

Ex vivo analysis

BxPC3 xenografts were excised and one each was either embedded in Tissue–Plus OCT compound and frozen on dry ice or fixed with 4% paraformaldehyde (PFA) solution and subsequently sectioned (10 μm). Masson's trichrome staining, autoradiography, and anti-CA19.9 immunofluorescence staining were performed on sequential sections as previously described (Fig. 4C; refs.29, 31). Further details may be found in Supplementary Information.

Statistical analysis

To analyze the effect of therapy within each cohort, the therapeutic response was assessed using a random effect model (33). In this model it is assumed that the log volume–time profile of

Table 1. Absorbed doses and therapeutic indices calculated using the biodistribution data for ^{177}Lu-DOTA-PEG$_7$-Tz + 5B1-TCO

Target organ	Rad/mCi[a]	cGy/MBq	Therapeutic index
Tumor	20,571	556.0	—
Blood	1,804	48.8	11.4
Small intestine	126	3.4	163
Stomach	69.2	1.9	297
Large intestine	74.9	2.0	275
Heart	253	6.8	81.4
Kidneys	978	26.4	21.0
Liver	794	21.5	25.9
Lungs	835	22.6	24.6
Muscle	138	3.7	149
Bone	307	8.3	67.0

[a]Mean organ absorbed doses and effective dose are expressed in rad/mCi and rem/mCi.

Table 2. Dosimetry and absorbed dose estimations for 70 kg Standard Man model calculated from the biodistribution data for ^{177}Lu-DOTA-PEG$_7$-Tz + 5B1-TCO in a murine xenograft model

			Absorbed dose (rad) – 70 kg human	
Organ	**rad/mCi[a]**	**cGy/MBq**	**150 mCi**	**700 mCi**
Adrenals	0.229	0.00619	34	160
Brain	0.222	0.00600	33	155
Breasts	0.215	0.00581	32	151
Gallbladder wall	0.231	0.00624	35	162
Lower long intestine wall	0.234	0.00632	35	164
Small intestine	0.282	0.00762	42	197
Stomach wall	0.235	0.00635	35	165
Upper long intestine wall	0.231	0.00624	35	162
Heart wall	0.263	0.00711	39	184
Kidneys	0.188	0.00508	28	132
Liver	0.229	0.00619	34	160
Lungs	0.223	0.00603	33	156
Muscle	0.156	0.00422	23	109
Ovaries	0.230	0.00622	35	161
Pancreas	0.230	0.00622	35	161
Red marrow	0.213	0.00576	32	149[b]
Osteogenic cells	0.982	0.02654	147	687
Skin	0.211	0.00570	32	148
Spleen	0.146	0.00395	22	102
Testes	0.220	0.00595	33	154
Thymus	0.223	0.00603	33	156
Thyroid	0.223	0.00603	33	156
Bladder wall	0.228	0.00616	34	160
Uterus	0.232	0.00627	35	162
Total body	0.280	0.00757	42	196
Effective dose	0.222	0.00600	33	155

[a]Mean organ absorbed doses and effective dose are expressed in rad/mCi and rem/mCi.
[b]Projected dose-limiting organ for PRIT is bone marrow (MTD $\sim$ 150 rad).

each mouse deviates in a random fashion from an average profile. The model for mouse i, in which μ is the average intercept, α_i is a random intercept (accounting for random effect) for each mouse, β is the slope (treatment effect over time), and c_i is a random error term, is

$$\log(\text{volume}_i) = \mu + \alpha_i + (\beta x \,\text{time}) + c_i.$$

Using a Likelihood ratio test, the above model was used to test for a significant change in log tumor volume over time, within each cohort and for pair-wise comparisons between cohorts. For each cohort, we use the above model to estimate the doubling or halving time and the delta method to calculate a 95% confidence interval for our estimate (34). All models were fit using the lme4 package in R version 3.1.1.

Results

Preparation and characterization of PRIT components

For this investigation, 5B1-TCO was synthesized via conjugation of the antibody with TCO-NHS and characterized *in vitro* as previously reported (23).

Radioligand precursors were successfully synthesized in three steps: the coupling of Tz-NHS and *O*-(2-aminoethyl)-*O*'-[2-(bocamino)ethyl]hexaethylene glycol to form Tz-PEG$_7$-NHBoc, the removal of the protecting group with TFA/CH_2Cl_2, and the ligation of Tz-PEG$_7$-NH$_2$ with either *p*-NCS-Bn-DOTA or *p*-NCS-Bn-CHX-A″-DTPA (Supplementary Fig. S1). In this way, Tz-PEG$_7$-CHX-A″-DTPA (1) and Tz-PEG$_7$-DOTA (2) were synthesized in 87% and 73% yield, respectively. In both cases, the chemical structure of all compounds was confirmed via ^{1}H-NMR (Supplementary Fig. S2), ^{13}C-NMR, ESI-MS, and HR-MS.

The chelator-modified tetrazines were radiolabeled via incubation with [^{177}Lu]-$LuCl_3$ for 10 minutes at 37°C in 250 mmol/L NH_4OAc, pH 5.5 (Supplementary Fig. S3). ^{177}Lu-CHX-A″-DTPA-PEG$_7$-Tz (**^{177}Lu-1**) was produced in >99% radionuclidic purity, 99.5% radiochemical yield, and a specific activity of 383 mCi/μmol ($n = 3$), whereas ^{177}Lu-DOTA-PEG$_7$-Tz (**^{177}Lu-2**) was produced in >96% radionuclidic purity, 96.9 ± 0.74% radiochemical yield, and a specific activity of 466 ± 155 mCi/μmol ($n = 3$).

Functional characterization of radioligands

The partition coefficients of the radioligands were determined using 1-octanol and PBS (pH 7.4), yielding values for the two hydrophilic compounds of −3.7 ± 0.1 for ^{177}Lu-DOTA-PEG$_7$-Tz and −3.2 ± 0.2 for ^{177}Lu- CHX-A″-DTPA-PEG$_7$-Tz. These values suggest that there is little difference in the hydrophobicity of the ligands. Stability assays revealed that both radioligands are quite stable, with >85% and >80% of each radioligand remaining intact after an incubation of 48 hours in PBS and serum, respectively (Supplementary Table S1). These rates of decomposition are unlikely to hamper the *in vivo* performance of the system, as the clearance half-times of the radioligands are short. Ultimately, owing to the similar physical properties and the relative ease of synthesis and purification, we chose to evaluate both radioligands in preliminary *in vivo* investigations.

Biodistribution

Biodistribution studies were performed with three goals in mind: (i) the identification of the appropriate dose of 5B1-TCO to give for PRIT in this xenograft model; (ii) a side-by-side comparison of both radioligands to determine the best candidate for *in vivo* PRIT studies; and (iii) the quantification of the uptake and clearance of the preferred radioligand for dosimetry calculations. We first performed a pilot study in which mice with BxPC3 xenograft-bearing mice were administered either 100 or 200 μg of 5B1-TCO, followed by 1.5 molar equivalents of ^{177}Lu-CHX-A″-DTPA-PEG$_7$-Tz. We chose to analyze only one radioligand for this study to reduce the number of animals needed. We found that administration of 200 μg of 5B1-TCO led to significantly better tumor accumulation and similar or even better tumor-to-tissue activity concentration ratios (Supplementary Fig. S4A and S4B), consistent with previously reported PET imaging studies using 5B1-TCO as a targeting vector (23, 24).

Next, we compared the two radioligands using the optimal amount of 5B1-TCO. This investigation showed that pretargeting with ^{177}Lu-DOTA-PEG$_7$-Tz produced significantly higher tumor activity concentrations than pretargeting with ^{177}Lu-CHX-A″-DTPA-PEG$_7$-Tz: 12.0 ± 5.3% ID/g and 4.3 ± 1.8% ID/g at 72-hour postinjection, respectively (Fig. 2; Supplementary Fig. S4C and S4D). This led us to choose the former for *in vivo* therapy studies. A final biodistribution was performed by administering 200 μg of 5B1-TCO followed 72 hours later by 1.5 molar equivalents of ^{177}Lu-DOTA-PEG$_7$-Tz and collecting tissues at five time points between 4 and 120 hours. The activity concentrations observed in the tumor tissue were high, reaching 16.8 ± 3.87% ID/g at 120 hours postinjection

(Fig. 2; Supplementary Fig. S5; and Supplementary Table S2). Clearance from background tissue was rapid, with all tumor-to-tissue activity concentration ratios exceeding 15:1 at 120 hours (Fig. 2, inset).

Dosimetry

The mean organ absorbed doses for mice and the extrapolation of this data to the 70 kg Standard Man model are reported in Tables 1 and 2, respectively. The ratio of the mean organ

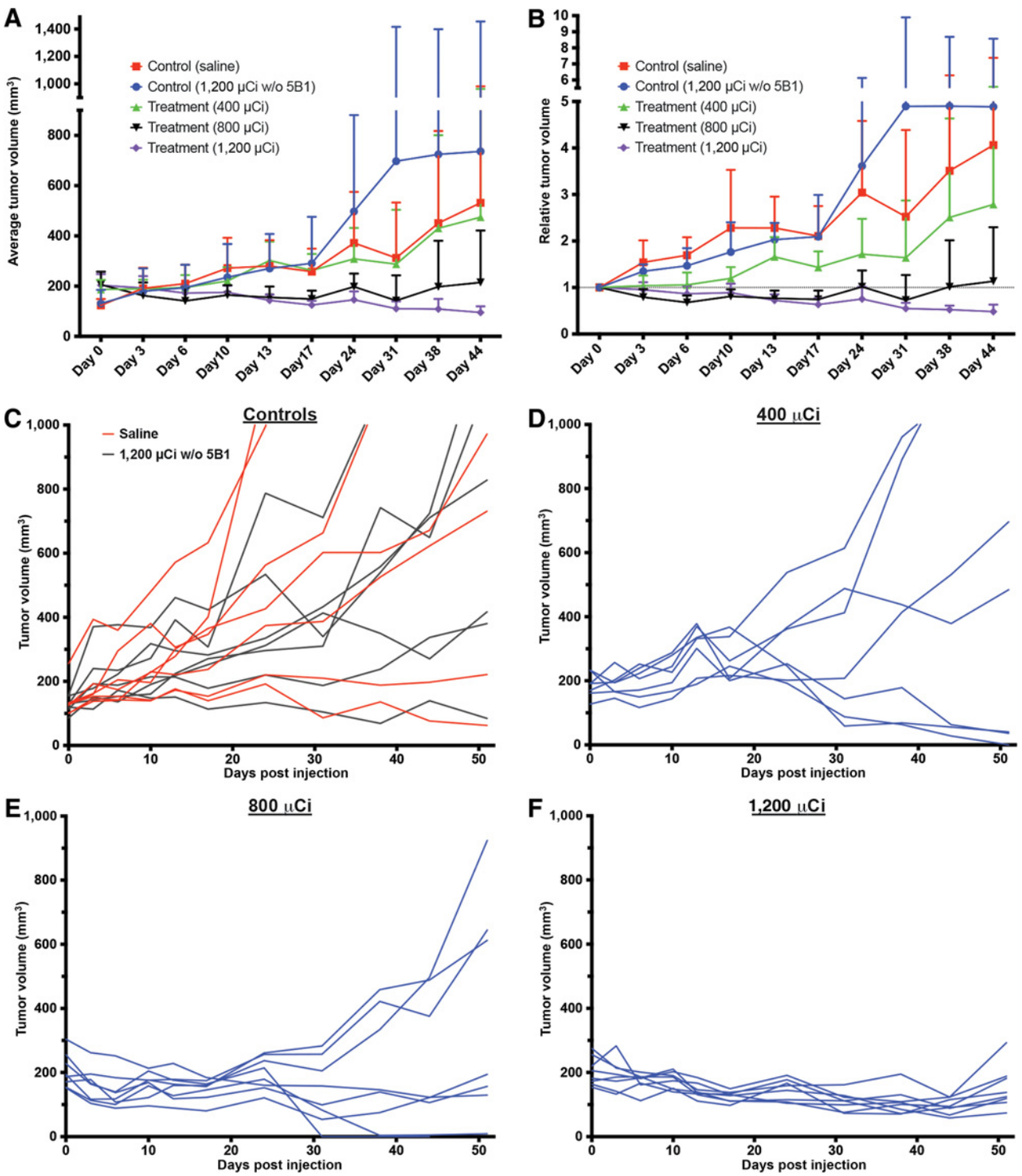

Figure 3.

Plots of the average tumor volume (**A**) and relative tumor volume (**B**) for each cohort of mice during the first 31 days of the PRIT study are shown with error bars denoting standard deviation. Line graphs mapping the response of each individual mouse over the entire course of the PRIT study are shown for the control groups (**C**) as well as each therapy cohort (**D–F**).

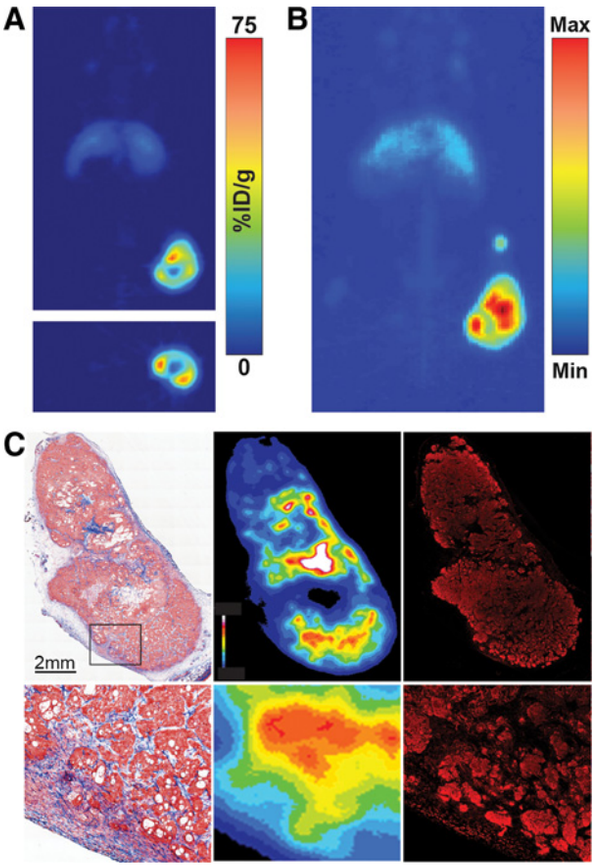

Figure 4.

Tomographic slices (**A**) and maximum intensity projections (**B**) of PET images (120-hour postinjection) of a mouse from the 800 μCi therapy cohort that was injected with ^{89}Zr-5B1 at the conclusion of the therapy study. Masson's trichrome (**C**, left), autoradiography (**C**, middle), and anti-CA19.9 immunofluorescence (**C**, right) on the excised tumor of the same mouse at the conclusion of the imaging study are also shown.

absorbed dose in mice relative to that to the tumor ("therapeutic index") is also reported. Calculating the absorbed dose in humans using the dosimetry data suggests that a 150 mCi administration of radioligand would not exceed the MTD in off-target tissues in humans. Assuming a MTD for red marrow of 150 rad, the maximum tolerated administered activity would be approximately 700 mCi (Table 2; refs.7, 35).

In vivo therapy

To establish dose response using the optimized PRIT protocol, mice ($n = 7–8$ per cohort) were administered 5B1-TCO 72 hours prior to the injection of 400, 800, or 1,200 μCi of ^{177}Lu-DOTA-PEG$_7$-Tz. Control groups were not administered 5B1-TCO and were instead injected either with vehicle or 1,200 μCi of ^{177}Lu-DOTA-PEG$_7$-Tz. One mouse from the 800 μCi therapy cohort was euthanized after 24 days due to an infection, although it is unclear whether this was event was related to the therapy study. No other mice showed any outward signs of toxicity, and all mice maintained an acceptable body weight (>80% original weight) throughout the course of the study. Average weight loss for any cohort never exceeded 6%, and there was not any significant difference among any of the therapy or control cohorts at any time point. These results suggest that the treatment was well tolerated up to the highest administered therapeutic dose of 1,200 μCi.

Following the average tumor volume for the first 31 days after treatment clearly shows a differential response that improves (more dramatic growth delay or shrinkage) with increasing ^{177}Lu activity in the therapy cohorts (Fig. 3A and B). Analysis of the growth-delay effects across each cohort becomes convoluted after that point, as mice with tumors >1,000 mm^3 are removed from that point on. As of 51 days posttreatment, 75% (6/8) of the mice from the therapy cohort receiving 1,200 μCi of ^{177}Lu-DOTA-PEG$_7$-Tz had tumors that were smaller than they had been on day 1.

A subjective analysis of the average tumor volume and relative tumor volume measurements (Fig. 3A and B) suggested therapeutic efficacy in both the 800 and 1,200 μCi therapy cohorts, which was sustained until the endpoint of the experiment. Some heterogeneity in response within cohorts was observed, especially for the 800-μCi cohort, as depicted by the line graphs following each individual mouse (Fig. 3C–F). This may be attributed to variations in the CA19.9 expression among tumors or differences in tumor volumes at the beginning of the study. To account for that variance and objectively examine the data over the course of the entire study, the data were analyzed using a random effect model (Supplementary Table S3). The statistical analysis showed that the therapeutic response was statistically significant for the 1,200-μCi cohort relative to both controls and the 400-μCi cohort.

PET imaging

^{89}Zr-5B1 PET images acquired in 6 selected mice at the conclusion of the *in vivo* PRIT study all showed demonstrable uptake of the tracer in tumor (Fig. 4A and B; Supplementary Fig. S7). The mice that received PRIT showed marginally higher uptake of the tracer in the tumor at 120-hour postinjection relative to the controls, although no conclusions as to the cause of that increase can be drawn due to the small sample size.

Ex vivo analysis

Ex vivo analysis of ^{89}Zr-5B1 distribution via autoradiography revealed a nonuniform microscopic distribution of the tracer within the tumor. The areas of highest activity concentration were observed to be close to regions with a higher density of tumor stroma (Fig. 4C), which most likely indicates delivery of the radiotracer via the tumor vasculature. Diffusion of ^{89}Zr-5B1 from these sites is also observed, and association with regions of 5B1 expression (Fig. 4C) is also seen. This uptake pattern of the radiotracer can be explained by a combination of slow diffusion from the site of vascular delivery and the high-affinity binding of ^{89}Zr-5B1 to local sites of high CA19.9 that prevents further tumor penetration. Minimal uptake of ^{89}Zr-5B1 was observed in regions of central tumor necrosis.

Discussion

Our approach to PRIT is based on our previously reported strategy for the pretargeted PET imaging of PDAC (23). The system employed two components, a ^{64}Cu-labeled tetrazine radioligand (^{64}Cu-Tz-PEG$_7$-NOTA) and a trans-cyclooctene–conjugated 5B1 antibody (5B1-TCO). 5B1 is a fully human mAb that targets carbohydrate antigen 19.9 (CA19.9), a cell surface antigen and a biomarker that has shown clinical value for the diagnosis,

staging, and prognostic evaluation of pancreatic cancer. Critically, our results demonstrate that the delineation of CA19.9-expressing tissues via pretargeted PET is possible despite the shedding of CA19.9 from cells and the moderate internalization rates of 5B1 after binding its antigen (23). Not surprisingly; however, a shift in the structure of the radioligand was needed. The β-emitting lanthanide $^{177}Lu^{3+}$ ($t_{1/2} \sim 6.7$ days) requires a different chelator than the divalent $^{64}Cu^{2+}$ ($t_{1/2} \sim 12.7$ hours) that was used for the PET imaging system. As a result, two novel tetrazine-bearing radioligands were designed for the current project, ^{177}Lu-DOTA-PEG$_7$-Tz and ^{177}Lu-CHX-A″-DTPA-PEG$_7$-Tz (Fig. 1C). These two constructs each employ a well-characterized and clinically validated chelator for $^{177}Lu^{3+}$-DOTA and CHX-A″-DTPA-as well as a PEG$_7$ linker and Tz functionality. The inclusion of the PEG$_7$ linker in this type of molecule has been shown to expedite hepatobiliary clearance while maintaining the capability of similar radioligands to target TCO-conjugated biomolecules in tumor tissues.

The two radioligands that we assessed, ^{177}Lu-DOTA-PEG$_7$-Tz and ^{177}Lu-CHX-A″-DTPA-PEG$_7$-Tz, did not produce equal tumor activity concentrations in pretargeting experiments with 5B1-TCO. Indeed, our pilot biodistribution studies in mice with BxPC3 xenografts indicated that pretargeting with ^{177}Lu-DOTA-PEG$_7$-Tz and 5B1-TCO produced higher tumor activity concentrations at 72-hour postinjection than pretargeting with ^{177}Lu-CHX-A″-DTPA-PEG$_7$-Tz and 5B1-TCO (Supplementary Fig. S3). The trends in the biodistribution data do not offer a definitive explanation for the superior performance of the DOTA-bearing radioligand compared to its CHX-A″-DTPA-modified counterpart, but the latter did show a modest increase in retention in the large intestine and kidneys (Supplementary Fig. S4). Furthermore, the stability and log D studies do little to shed any additional light on the differing uptake of the two ligands. As may have been expected, the radioligand with the cyclic chelator DOTA showed slightly higher stability in serum (Supplementary Table S1), but this would likely not account for the >2.5-fold increase in tumor activity concentrations observed in the pretargeting biodistribution experiments. Despite the lack of a cogent explanation for the differential behavior of these two radioligands, ^{177}Lu-DOTA-PEG$_7$-Tz was chosen for more thorough *in vivo* biodistribution, dosimetry, and, most importantly, therapy studies.

Further biodistribution studies in which ^{177}Lu-DOTA-PEG$_7$-Tz was injected 72 hours after the administration of 5B1-TCO confirmed the high uptake and, perhaps more importantly, long retention of radioactivity in tumor tissue up to 5 days postinjection (Fig. 2). Clearance from nontarget tissues was rapid and led to remarkably high tumor-to-normal tissue activity concentration ratios at 120 hours (Fig. 2, inset). The gradually increasing uptake and long retention seen with this system are an advantage over other PRIT systems that rely solely on noncovalent interactions between radioligands and immunoconjugates. Ligands that rely on such interactions may clear from tumor tissue in a matter of hours after reaching maximal uptake. Of course, this is not ideal when using an isotope (e.g., ^{177}Lu) that delivers its radioactive payload over the course of weeks. By covalently linking the radioligand to the targeting vector, in this case 5B1-TCO, and achieving a rapid clearance from nontarget tissues, a higher proportion of the injected activity may be delivered to the tumor tissue while minimizing the risk of radiogenic toxicity in nontarget tissues.

The dosimetry estimations for a 70 kg Standard Man model suggest that our PRIT approach may efficiently deliver cytotoxic radiation to tumor tissues without causing significant side-effects in humans. The most common dose-limiting tissue in RIT is the red marrow, the maximum tolerated dose being approximately 150 cGy (7). Organs that are typically associated with the clearance of antibody-based agents are the kidneys, liver, and spleen, and those organs can typically tolerate doses of greater than 1,500 cGy (7, 35). The data indicate that with a single administration of 200 mCi (7,400 MBq) of radioligand, the predicted maximum tolerated dose in any off-target tissue would not be reached (Table 2). In our estimation, the MTD in humans would be reached at a dose of approximately 700 mCi (25,900 MBq), with the dose-limiting organ most likely being the red marrow (Table 2). Although it is not possible to reliably predict the radiation dose and resulting therapeutic response in human tumors, a retrospective evaluation of previous RIT approaches, both directly targeted and pretargeted, indicates that our approach meets or exceeds the dose benchmarks in preclinical murine models that would likely be necessary to achieve a therapeutic response in humans.

Previously reported PRIT systems have introduced a clearing agent via an additional injection between those of the targeting vector and the radioligand. The function of the clearing agent is to reduce the amount of accessible binding or reactive sites on the targeting vector that is still circulating in the blood at the time of radioligand injection, thus reducing the dose to sensitive, nontarget organs such as the red marrow from the subsequent injection of the radioligand. Based on our biodistribution and dosimetry results, our system may not require the use of a clearing agent, an added advantage over other systems. Previous studies have nonetheless shown that clearing agents are effective in the context of TCO- and Tz-based imaging systems (26), and this approach could certainly be adopted in the future if necessary.

PRIT studies confirmed that our approach was effective in causing significant growth delay and even regression of BxPC3 xenografts at the two highest activities tested, whereas the growth delay observed with the lowest activity (400 μCi) was not statistically significant. Although detailed statistical analysis of each cohort is complicated as mice from each cohort began to reach the endpoint, the trend is clear, and statistical significance was rapidly achieved in the control groups and both the 800- and 1,200-μCi cohorts.

Interestingly, line graphs (Fig. 3C–F) depicting the tumor size of each individual mouse within a cohort show that, perhaps with the exception of the 1,200 μCi therapy cohort, not all tumors within a particular cohort responded in a similar manner. This is likely due to differences in the initial uptake of the 5B1-TCO, the heterogeneity of CA19.9 expression, and the tumor sizes. We have observed this same variation in uptake in BxPC3 xenografts with a number of 5B1-based radiotracers in the past (23, 29, 31). In fact, heterogeneity is a common characteristic of many types of human malignancies, especially PDAC. Although no quantitative PET imaging was carried out prior to the initiation PRIT in this study, we believe that ^{89}Zr-5B1, which is currently being evaluated in clinical trials for patients with PDAC, may be useful as a diagnostic tool.

The results of the post-PRIT PET imaging study with ^{89}Zr-5B1 (Fig. 4A; Supplementary Fig. S7) suggest that CA19.9 expression persists posttherapy in tumors that remain viable after treatment. This suggests that ^{89}Zr-5B1 PET imaging could be used to monitor

therapeutic response as well as to determine whether a patient may potentially be responsive to multiple administrations of fractionated PRIT. Pretargeted PET imaging with recently reported ^{18}F- or ^{64}Cu-labeled Tz ligands would likely also be effective. Using pretargeted imaging with short-lived isotopes would rapidly provide high-quality images while reducing the radiation dose to healthy tissues. Using the pretargeted imaging approach would also provide a more straightforward assessment of the possibility of delivering additional cytotoxic radiation to the tumors via additional rounds of PRIT. Each of these potential theranostic approaches are currently being investigated in murine models of PDAC.

Ex vivo analysis showed that delivery of 5B1-based imaging and therapy agents may be limited by diffusion and trapping of the agents by areas of high CA19.9 density near sites of vascular delivery. It is likely that adjustments to the specific activity and/or injected mass of 5B1 could influence this distribution, as could the length of time allowed between administration and assessment. PDAC tumors are known for their dense desmoplastic stroma, and tumor penetration may well be a concern in the translation of antibody-based PRIT. However, this constraint may be alleviated by the use of compounds that act to increase stromal permeability (36). Further studies to evaluate the effectiveness of such an approach are currently underway in our laboratory.

In conclusion, our *in vivo* therapy results have shown that our bioorthogonal pretargeting system utilizing Tz-based radioligands and TCO-modified immunoconjugates is a promising platform for the development of PRIT systems. It is important to note that the inherent complexity of pretargeted immunotherapy can create complications as we move toward the clinic. Indeed, the translation and clinical optimization of a multicomponent system will undoubtedly be more cumbersome than analogous approaches that utilize a single agent. Nonetheless, we are confident that the benefits of our PRIT strategy, and especially future generations, will outweigh any logistical drawbacks. Along these lines, we believe that this platform warrants further optimization and a number of prospective routes could lead to improved results. For example, previous studies on PRIT systems that use a fractionated dosing schedule have shown promise, with some demonstrating equal absorbed doses in nontarget organs and significant improvements in response rates compared to a single administration of the radioligand. Our laboratories are currently working to establish MTD in preparation for fractioned PRIT studies using the system reported herein. In addition, in future experiments we will assess the ability of 5B1-based PET imaging to quantify CA19.9 levels prior to therapy in order to evaluate ^{89}Zr-5B1 as a theranostic tool for predicting response to 5B1-based PRIT.

Disclosure of Potential Conflicts of Interest

No potential conflicts of interest were disclosed.

Authors' Contributions

Conception and design: J.L. Houghton, W.W. Scholz, J.S. Lewis, B.M. Zeglis
Development of methodology: J.L. Houghton, S. Carlin, J.S. Lewis, B.M. Zeglis
Acquisition of data (provided animals, acquired and managed patients, provided facilities, etc.): J.L. Houghton, R. Membreno, D. Abdel-Atti, S. Carlin
Analysis and interpretation of data (e.g., statistical analysis, biostatistics, computational analysis): J.L. Houghton, R. Membreno, K.M. Cunanan, S. Carlin, W.W. Scholz, P.B. Zanzonico, J.S. Lewis
Writing, review, and/or revision of the manuscript: J.L. Houghton, R. Membreno, D. Abdel-Atti, W.W. Scholz, P.B. Zanzonico, J.S. Lewis, B.M. Zeglis
Administrative, technical, or material support (i.e., reporting or organizing data, constructing databases): R. Membreno, D. Abdel-Atti, J.S. Lewis
Study supervision: J.S. Lewis, B.M. Zeglis

Acknowledgments

We would like to thank the staff of the Small Animal Imaging Core Facility, the Radiochemistry and Molecular Imaging Probe Core Facility, Mr. William H. and Alice Goodwin and the Commonwealth Foundation for Cancer Research, and The Center for Experimental Therapeutics at MSKCC.

Grant Support

The MSKCC Small Animal Imaging Core Facility as well as the Radiochemistry and Molecular Imaging Probe core were supported in part by NIH grant P30 CA08748. J.L. Houghton received 1F32CA180452-01A1 and 5R25CA096945-09. W.W. Scholz received 2R42CA128362 and HHSN261201300060C. B.M. Zeglis received 1K99CA178205-01A1 and 4R00CA178205-02. All experiments were supported by The Experimental Therapeutics Center at MSKCC.

The costs of publication of this article were defrayed in part by the payment of page charges. This article must therefore be hereby marked advertisement in accordance with 18 U.S.C. Section 1734 solely to indicate this fact.

Received August 2, 2016; revised October 20, 2016; accepted November 1, 2016; published OnlineFirst November 9, 2016.

References

1. Goldenberg DM.Targeted therapy of cancer with radiolabeled antibodies. J Nucl Med 2002;43:693–713.
2. Jurcic JG, Larson SM, Sgouros G, McDevitt MR, Finn RD, Divgi CR, et al. Targeted α particle immunotherapy for myeloid leukemia. Blood 2002; 100:1233–9.
3. Kaminski MS, Estes J, Zasadny KR, Francis IR, Ross CW, Tuck M, et al. Radioimmunotherapy with iodine (131)I tositumomab for relapsed or refractory B-cell non-Hodgkin lymphoma: updated results and long-term follow-up of the University of Michigan experience. Blood 2000; 96:1259–66.
4. Witzig TE, Gordon LI, Cabanillas F, Czuczman MS, Emmanouilides C, Joyce R, et al. Randomized controlled trial of yttrium-90-labeled ibritumomab tiuxetan radioimmunotherapy versus rituximab immunotherapy for patients with relapsed or refractory low-grade, follicular, or transformed B-cell non-Hodgkin's lymphoma. J Clin Oncol 2002;20:2453–63.
5. Ugur O, Kostakoglu L, Hui ET, Fisher DR, Garmestani K, Gansow OA, et al. Comparison of the targeting characteristics of various radioimmunoconjugates for radioimmunotherapy of neuroblastoma: dosimetry calculations incorporating cross-organ beta doses. Nucl Med Biol 1996;23:1–8.
6. Huang CY, Pourgholami MH, Allen BJ. Optimizing radioimmunoconjugate delivery in the treatment of solid tumor. Cancer Treat Rev 2012; 38:854–60.
7. Larson SM, Carrasquillo JA, Cheung NK, Press OW. Radioimmunotherapy of human tumours. Nat Rev Cancer 2015;15:347–60.
8. Viola-Villegas NT, Sevak KK, Carlin SD, Doran MG, Evans HW, Bartlett DW, et al. Noninvasive Imaging of PSMA in prostate tumors with (89)Zr-Labeled huJ591 engineered antibody fragments: the faster alternatives. Mol Pharm 2014;11:3965–73.
9. Watanabe R, Hanaoka H, Sato K, Nagaya T, Harada T, Mitsunaga M, et al. Photoimmunotherapy targeting prostate-specific membrane antigen: are antibody fragments as effective as antibodies? J Nucl Med 2015;56:140–4.
10. Frampas E, Rousseau C, Bodet-Milin C, Barbet J, Chatal JF, Kraeber-Bodere F. Improvement of radioimmunotherapy using pretargeting. Front Oncol 2013;3:159.
11. Cheal SM, Xu H, Guo HF, Zanzonico PB, Larson SM, Cheung NK. Preclinical evaluation of multistep targeting of diasialoganglioside GD2 using an IgG-scFv bispecific antibody with high affinity for GD2 and DOTA metal complex. Mol Cancer Ther 2014;13:1803–12.

12. Kraeber-Bodere F, Rousseau C, Bodet-Milin C, Ferrer L, Faivre-Chauvet A, Campion L, et al. Targeting, toxicity, and efficacy of 2-step, pretargeted radioimmunotherapy using a chimeric bispecific antibody and 131I-labeled bivalent hapten in a phase I optimization clinical trial. J Nucl Med 2006;47:247–55.
13. Mallikaratchy P, Gardner J, Nordstrom LU, Veomett NJ, McDevitt MR, Heaney ML, et al. A self-assembling short oligonucleotide duplex suitable for pretargeting. Nucleic Acid Ther 2013;23:289–99.
14. Mohsin H, Jia F, Bryan JN, Sivaguru G, Cutler CS, Ketring AR, et al. Comparison of pretargeted and conventional CC49 radioimmunotherapy using 149Pm, 166Ho, and 177Lu. Bioconjugate Chem 2011;22:2444–52.
15. Pagel JM, Kenoyer AL, Back T, Hamlin DK, Wilbur DS, Fisher DR, et al. Anti-CD45 pretargeted radioimmunotherapy using bismuth-213: high rates of complete remission and long-term survival in a mouse myeloid leukemia xenograft model. Blood 2011;118:703–11.
16. Blackman ML, Royzen M, Fox JM. Tetrazine ligation: fast bioconjugation based on inverse-electron-demand diels−alder reactivity. J Am Chem Soc 2008;130:13518–9.
17. Reiner T, Zeglis BM. The inverse electron demand Diels-Alder click reaction in radiochemistry. J Labelled Comp Radiopharm 2014;57:285–90.
18. Devaraj NK, Upadhyay R, Haun JB, Hilderbrand SA, Weissleder R. Fast and sensitive pretargeted labeling of cancer cells through a tetrazine/trans-cyclooctene cycloaddition. Angewandte Chemie 2009;48:7013–6.
19. Rossin R, van den Bosch SM, Ten Hoeve W, Carvelli M, Versteegen RM, Lub J, et al. Highly reactive trans-cyclooctene tags with improved stability for Diels-Alder chemistry in living systems. Bioconjugate Chem 2013;24:1210–7.
20. Rossin R, van Duijnhoven SM, Lappchen T, van den Bosch SM, Robillard MS. Trans-cyclooctene tag with improved properties for tumor pretargeting with the diels-alder reaction. Mol Pharm 2014;11:3090–6.
21. Zeglis BM, Sevak KK, Reiner T, Mohindra P, Carlin SD, Zanzonico P, et al. A pretargeted PET imaging strategy based on bioorthogonal Diels-Alder click chemistry. J Nucl Med 2013;54:1389–96.
22. Rossin R, Verkerk PR, van den Bosch SM, Vulders RC, Verel I, Lub J, et al. In vivo chemistry for pretargeted tumor imaging in live mice. Angewandte Chemie 2010;49:3375–8.
23. Houghton JL, Zeglis BM, Abdel-Atti D, Sawada R, Scholz WW, Lewis JS. Pretargeted immuno-PET of pancreatic cancer: overcoming circulating antigen and internalized antibody to reduce radiation doses. J Nucl Med 2016;57:453–9.
24. Meyer JP, Houghton JL, Kozlowski P, Abdel-Atti D, Reiner T, Pillarsetty NV, et al. (18)F-Based pretargeted PET imaging based on bioorthogonal diels-alder click chemistry. Bioconjugate Chem 2016;27:298–301.
25. Zeglis BM, Brand C, Abdel-Atti D, Carnazza KE, Cook BE, Carlin S, et al. Optimization of a pretargeted strategy for the PET imaging of colorectal carcinoma via the modulation of radioligand pharmacokinetics. Mol Pharm 2015;12:3575–87.
26. Rossin R, Lappchen T, van den Bosch SM, Laforest R, Robillard MS. Diels-Alder reaction for tumor pretargeting: in vivo chemistry can boost tumor radiation dose compared with directly labeled antibody. J Nucl Med 2013;54:1989–95.
27. Rossin R, Robillard MS. Pretargeted imaging using bioorthogonal chemistry in mice. Curr Opin Chem Biol 2014;21:161–9.
28. van Duijnhoven SM, Rossin R, van den Bosch SM, Wheatcroft MP, Hudson PJ, Robillard MS. Diabody pretargeting with click chemistry in vivo. J Nucl Med 2015;56:1422–8.
29. Viola-Villegas NT, Rice SL, Carlin S, Wu X, Evans MJ, Sevak KK, et al. Applying PET to broaden the diagnostic utility of the clinically validated CA19.9 serum biomarker for oncology. J Nucl Med 2013;54:1876–82.
30. Girgis MD, Kenanova V, Olafsen T, McCabe KE, Wu AM, Tomlinson JS. Anti-CA19–9 diabody as a PET imaging probe for pancreas cancer. J Surg Res 2011;170:169–78.
31. Houghton JL, Zeglis BM, Abdel-Atti D, Aggeler R, Sawada R, Agnew BJ, et al. Site-specifically labeled CA19.9-targeted immunoconjugates for the PET, NIRF, and multimodal PET/NIRF imaging of pancreatic cancer. Proc Natl Acad Sci US A 2015;112:15850–5.
32. Stabin MG, Sparks RB, Crowe E. OLINDA/EXM: the second-generation personal computer software for internal dose assessment in nuclear medicine. J Nucl Med 2005;46:1023–7.
33. Pinheiro JC, Bates DM. Mixed-effects models in S and S-PLUS. New York, NY: Springer; 2000.
34. Casella G, Berger RL. Statistical inference. 2nd ed. Pacific Grove, CA: Thomson Learning; 2002.
35. Emami B, Lyman J, Brown A, Coia L, Goitein M, Munzenrider JE, et al. Tolerance of normal tissue to therapeutic irradiation. Int J Radiat Oncol Biol Phys 1991;21:109–22.
36. Whatcott CJ, Han H, Posner RG, Hostetter G, Von Hoff DD. Targeting the tumor microenvironment in cancer: why hyaluronidase deserves a second look. Cancer Discov 2011;1:291–6.